





Article

Influence of Supports on the Low-Velocity Impact Response of Square RC Slab of Standard Concrete and Ultra-High Performance Concrete: FEM-Based Computational Analysis

S. M. Anas ^{1,*}, Mohd Shariq ¹, Mehtab Alam ², Ahmed M. Yosri ^{3,*}, Ahmed Mohamed ⁴
and Mohamed AbdelMongy ^{3,5}

- ¹ Department of Civil Engineering, Jamia Millia Islamia (A Central University), New Delhi 110025, India; mohd1909933@st.jmi.ac.in
- ² Department of Civil Engineering, Netaji Subhas University of Technology, New Delhi 110073, India; mehtab.alam@nsut.ac.in
- ³ Department of Civil Engineering, College of Engineering, Jouf University, Sakakah 72388, Saudi Arabia; mfelmongy@ju.edu.sa
- ⁴ Structural Engineering and Construction Management, Future University in Egypt, New Cairo 11835, Egypt; ahmed.deifalla@fue.edu.eg
- ⁵ Civil Engineering Department, Faculty of Engineering, Al-Azhar University, Cairo 11651, Egypt
- * Correspondence: s1910521@st.jmi.ac.in (S.M.A.); amyosri@ju.edu.sa (A.M.Y.); Tel.: +91-8527764166 (S.M.A.)

Abstract: Structural members with low-flexural stiffness, such as slabs, are more susceptible to impulsive loadings induced by falling machines/tools during construction and installation, and also from rolling boulders/rocks triggered by wind/earthquake, especially in mountainous areas. The impact resistance of reinforced concrete (RC) slabs supported on two opposite edges (often called the one-way slab) and on all four edges (i.e., two-way slab) has been adequately studied experimentally as well as computationally, and is available in the literature. However, the slabs supported on three edges have not been studied under low-velocity impact for their impact response. For this purpose, a computational study is performed through finite elements by implementing ABAQUS software on the validated model, resulting in the slab, which is supported on (i) three edges and (ii) two opposite edges, to be subjected to low-velocity impact, induced by dropping a 105 kg non-deformable steel mass from a height of 2500 mm onto the slab centroid. Furthermore, the role of the material strength of the concrete of the slab is investigated via replacing the ultra-high performance concrete (UHPC) for standard or normal-strength concrete (NSC). The impact load is modeled by considering the explicit module of the software. Failure mechanism, stress/strain contour, displacement distribution, and crack pattern of the slabs are compared and discussed.

Keywords: failure modes; finite element method (FEM); damage; low-velocity impact; impact loading; RC slabs; simulations; supports effects; UHPC



Citation: Anas, S.M.; Shariq, M.; Alam, M.; Yosri, A.M.; Mohamed, A.; AbdelMongy, M. Influence of Supports on the Low-Velocity Impact Response of Square RC Slab of Standard Concrete and Ultra-High Performance Concrete: FEM-Based Computational Analysis. *Buildings* **2023**, *13*, 1220. <https://doi.org/10.3390/buildings13051220>

Academic Editor: David Arditi

Received: 25 January 2023

Revised: 15 February 2023

Accepted: 28 April 2023

Published: 5 May 2023



Copyright: © 2023 by the authors. Licensee MDPI, Basel, Switzerland. This article is an open access article distributed under the terms and conditions of the Creative Commons Attribution (CC BY) license (<https://creativecommons.org/licenses/by/4.0/>).

1. Introduction

Impulsive loading has many facets, of which, one is impact, where structural impact is a collision between a striking object and a target structure [1–3]. If a striking object during the impact deforms significantly, then it is referred to as “soft or mild impact”, and if the striking object undergoes little deformation, the impact is “hard or strong”. The impact is also classified as low-velocity impact (≤ 15 m/s) or high-velocity impact [2,3]. The target structure does not need to be stationary, for instance, two closely spaced building structures impact each other under earthquake or wind excitations. A phenomenon known as high-rate impact loading is generally caused by the transfer of a large amount of energy in a short duration of time and can be induced by intentional explosions, the falling of heavy machine tools during construction, and aircraft/vehicle collision [1–3].

With little ductility, concrete displays softening characteristics after attaining pre-compression, and the rate of loading makes an impact on the response of concrete [1–3]. Material resistance of concrete rises with change in its mode of failure with an increasing rate of loading [1–3]. Depending upon the target structure, location, and kind of impact, a high rate of loading on concrete structural elements results from one mode of failure to more modes [1–3].

To ascertain the resilience of lifeline buildings and public infrastructures against impulsive loadings is a pressing concern for developing countries [1–3]. Experimental facilities to study the material behavior and structural response are not commonly available. Moreover, the simulation of the nonlinear problems involving the modeling of material behavior under such high-rate loadings is not straightforward; therefore, research on structures subjected to impact loading still seems to be in a state of infancy [1–3].

Impact-loaded RC slabs typically undergo a localized failure in terms of punching, cracking, spalling, and scabbing of concrete [1–3]. When an object collides with the target structure, stress waves, including shear, longitudinal, and flexural ones, are generated, which proliferate from the area of impact toward the supports and the force-transferred rebounds by the inertia effect [1–3]. Lately, during impact, inertial influence diminishes and does not affect the dynamic response of the structure [1–3].

In comparison to the analytical approach, the experimental method is more instinctive and capable of providing the groundwork for theoretical/analytical investigations and computational simulations. Eight slabs were subjected to low-velocity impact tests in an experimental study by Ozgur et al. [4] to examine the influence of various support constraints. Kumar et al. [5] designed an impact test setup to compare the performance of the RC slab with the prestressed slab in terms of vertical deflection and acceleration. Li et al. [6], in a live explosion testing, investigated the failure mechanism of bidirectional slabs. Yao et al. [7] utilized 0.13 and 0.19 kg TNT charges to analyze the damage mechanism of RC slabs with varying percentages of steel reinforcement.

Additionally, using experimental techniques, various scholars [8–16] investigated the failure mode and mechanism of structural concrete members under drop load impact. Research works conducted by the authors of [17–20] are known as some recent instances of low-velocity impact research, where the samples tested experienced beyond point-of-impact damage. Even for these research, damage greatly continued to be local, and the perforation of the samples appeared to be a common incidence. Subsequently, outcomes of these kinds of research are not commonly accepted for more general low-velocity accidental impacts, including vehicle destruction, where the target of destruction responds to the impact globally as a structure, and therefore experiences great devastation, which happens to be beyond the point of impact.

Field and laboratory tests are the most popular direct approaches for analyzing the impact behavior of structural members. Observations as well as results from these tests not only demonstrate the performance of the members, but are also utilized in validating models created using commercial tools or codes [1–3]. However, live testing of the structural members is often avoided by the researchers, owing to high equipment and labor costs, as well as material costs and the possibility of serious injuries to the laboratory members. As there have been endless advancements in test technologies and computer simulations, scholars are utilizing publicly accessible commercial programs or tools to perform simulations of structural members subjected to impulsive and high-intense loadings. Numerical results allow users to understand the load-carrying mechanism and propagation of stress waves generated out of such loadings in the materials of the structures. Computer simulations, however, can only be employed when the model has been shown to produce accurate predictions. Ozbolt and Sharma [21] simulated the 3D RC beams that had varying shear reinforcement ratios to analyze the impact of strain rate on the rigidity, strength, as well as flexibility of the RC beams. The outcome of the study showed that the rate-sensitive microplane model strongly simulated the impact of the mechanical response of the RC beams. In another study, which was conducted by Lee et al. [22,23], the high-speed impact

course of the FRP-RC slab, as well as the steel fiber RC slab, were simulated using the finite element method software, and a conclusion was drawn which showed that the FRP and steel fibers are capable of diminishing the impact dynamic response in the plate, while also improving the impact resistance of the component. Zhao and Qian [24] created a 3D FE model of the earlier test and studied the effects of impact mass, span-depth ratio, and impact velocity on the impact behavior of RC beams. The analysis included the study of dynamic responses and dynamic shear capacity of the RC beams. Wang et al. [25], Yan et al. [26], Yankelevsky et al. [27], and Castedo et al. [28] conducted another simulation study to investigate the dynamic response of RC components, which also displayed the supremacy of numerical simulations in analyzing this issue. RC slabs having different layouts and ratios of the embedded reinforcement were analyzed by Othman and Marzouk [29] under low-impact loads. Energy absorption capacity and impulse were found unchanged with altering the layout and ratio of the embedded steel under similar impacts; however, the mode of failure and damage profile of the slab were greatly influenced by changing the reinforcement configuration and ratio. Another research work by the authors of [30] on steel-concrete slabs subjected to mild impact showed that slab resistance can be enhanced with a higher strength concrete (>50 MPa) and slab thickness (>100 mm) compared to increasing steel ratio or percentage. Jahami et al. [31] applied successive impact loads on a flat slab made of reinforced concrete and performed numerical simulations using the ABAQUS tool. Ordinary findings were reported, such as deflection, energy, and impulse, all of which increased with multiple impact loads on the slab. Song et al. [32] investigated how well metal tubes made of composites absorbed energy and responded to axial impacts.

Concrete structures during their construction or service life may experience high-rate impact loadings in the form of landslip hazards, intentional blasts, detonations, aircraft/vehicle collisions, and so on, as reported in [1–3,25–28,33]. Subsequently, since a very long time, researchers have been interested in the examination and in the designing of concrete structures that are exposed to impact loads [33]. However, because of its critical character in relation to the issue in military applications, research in this domain has instead been greatly focused on the examination and modeling against high-velocity impacts, such as the collision of a ballistic missile [33]. Corbett et al. [34] have compiled the results of several experimental investigations that have been conducted to examine the missile impact responses of structures. In these investigations, which featured the perforation of an RC plate by a missile impact, emphasis has been paid to understand the local behavior of the structural members, notably slabs. Furthermore, these tests used impacting missiles with velocities in the range of 15 to 100 m/s and tiny missile diameters in comparison to the thickness of the target element, which resulted in a highly localized behavior at the site of contact and minor damage to the area around it [34].

To the best of the authors' knowledge, no investigations related to the support effects on the impact response of RC slabs were conducted. Current research work focuses on understanding the failure mechanism under the low-velocity impact on RC slabs by reducing the number of supports with standard concrete (often called normal-strength concrete) and ultra-high performance concrete using the finite elements modeling approach coupled with the explicit dynamic analysis. Other research works conducted by Foraboschi [35–37] under concentrated static loads can be of interest to the readers.

The remainder of this numerical study is arranged as follows: Section 2 presents slab dimensions, embedded steel layout, finite elements, mesh size, constitutive mechanical models, damage simulation, general properties, mesh convergence, and other general settings used for simulations of the impact load on RC slabs; Section 3 discusses the results of the considered numerical models in terms of displacement, damage, stresses, and plastic strains; the load-carrying mechanism is also highlighted in this section; finally, Section 4 highlights major outcomes/findings of the study. Note that the modeling of successive impacts on the slab as well as eccentric impacts is not within the scope of this work. Materials of the impact test setup are idealized using mechanical constitutive models available in ABAQUS [38] following the reference experimental work considered [2,3,13].

Boundary/support conditions are also idealized following ref. [2,3,13]. Concrete has been modeled with CDP constitutive material model following [39,40]. Strain-rate effects on the material(s) properties are incorporated in the modeling by considering stress-increase factors (often called dynamic-increase factors) that are assumed constant, following the current literature, refs. [2,3,41–45]. Simulations are performed in ABAQUS [38] considering three modes, namely preprocessing, postprocessing, and visualization. Modeling, material properties, section assignment, supports, loadings, constraints, and interactions, all come under the preprocessing mode [38], whereas the postprocessor runs the process by employing a central difference explicit time integration algorithm. Visualization mode demonstrates the results in the form of plots and contours.

Impact load effects on structural components can be modeled or simulated with different numerical techniques (e.g., finite element, discrete element, computational fluid dynamics, etc.) available in various commercial codes or tools (e.g., ABAQUS, LS-DYNA, Air3D, ANSYS, etc.) [2,3,31,43–45]. The finite element approach is most commonly used by researchers and scholars owing to its simplicity and optimizing numerical convergence issues under such impulsive loading environments; the same has been considered in this work.

2. Numerical Modeling of RC Slabs under Drop Load Impact

Finite element (FE) modeling and incremental explicit analysis of the slabs under low-velocity impact are performed using the ABAQUS [38] tool. This software has been extensively employed in situations involving impulsive loading environments/scenarios [2,3,26,28,33] and similar material(s) response [1–3,28,33,34] in past numerical studies. Firstly, the slab that was experimentally analyzed by Sadraie et al. [13] is modeled, and the rationality of the FE model is examined in light of the experiment's recorded results from the literature. Then, the influence of support and the role of UHPC concrete on the impact behavior of the slab are investigated.

2.1. General Procedure

Referring to Figure 1, the impact test setup modeled in ABAQUS is identical to the one used by Sadraie et al. [13]. The setup consists of four parts: striker, RC slab (concrete and steel bars), and supporting steel beams and columns. The mesh model is shown in Figure 2. A rendered view of the slab with embedded bars is shown in Figure 3. The reinforcement drawing is represented in Figure 4. The C3D8R [38] (Figure 5a) entity element is chosen for concrete, striker, and supports. This element is mostly employed for nonlinear dynamic problems involving massive deformation by high-rate loadings. The B31 [38] (Figure 5b) entity element is selected for steel bars. The present simulation study involves six square RC slabs, $1000 \times 1000 \times 75 \text{ mm}^3$, shown in Figure 6. A control slab, designated as S-NSC-4s, is the same as tested by the authors of [13]. Noted that all of the slabs possess 0.88% tension steel reinforcement and are subjected to identical concentrated low-velocity drop load.

2.2. Assumptions Involved in the FE Modeling

The concrete damage plasticity (CDP) [2,3,38–40,46,47] material model is used for concrete. Past studies [2,3,26,43,45] showed that this model is capable of accurately simulating the flexural and shear responses of RC members subjected to low-velocity impact loading. Furthermore, concrete damping as well as stiffness degradation and softening effects are considered in the CDP model. Stress and inelastic strain of the concrete are linked together by scalar damage coefficients as given in Equation (1), where E_c = concrete modulus, σ = stress, ε = strain, ε^{pl} = plastic strain, and d = damage coefficients (0.0–1.0).

$$\begin{cases} \sigma_c = E_c (\varepsilon_c - \varepsilon_c^{pl}) (1 - d_c) \\ \sigma_t = E_c (\varepsilon_t - \varepsilon_t^{pl}) (1 - d_t) \end{cases} \quad (1)$$

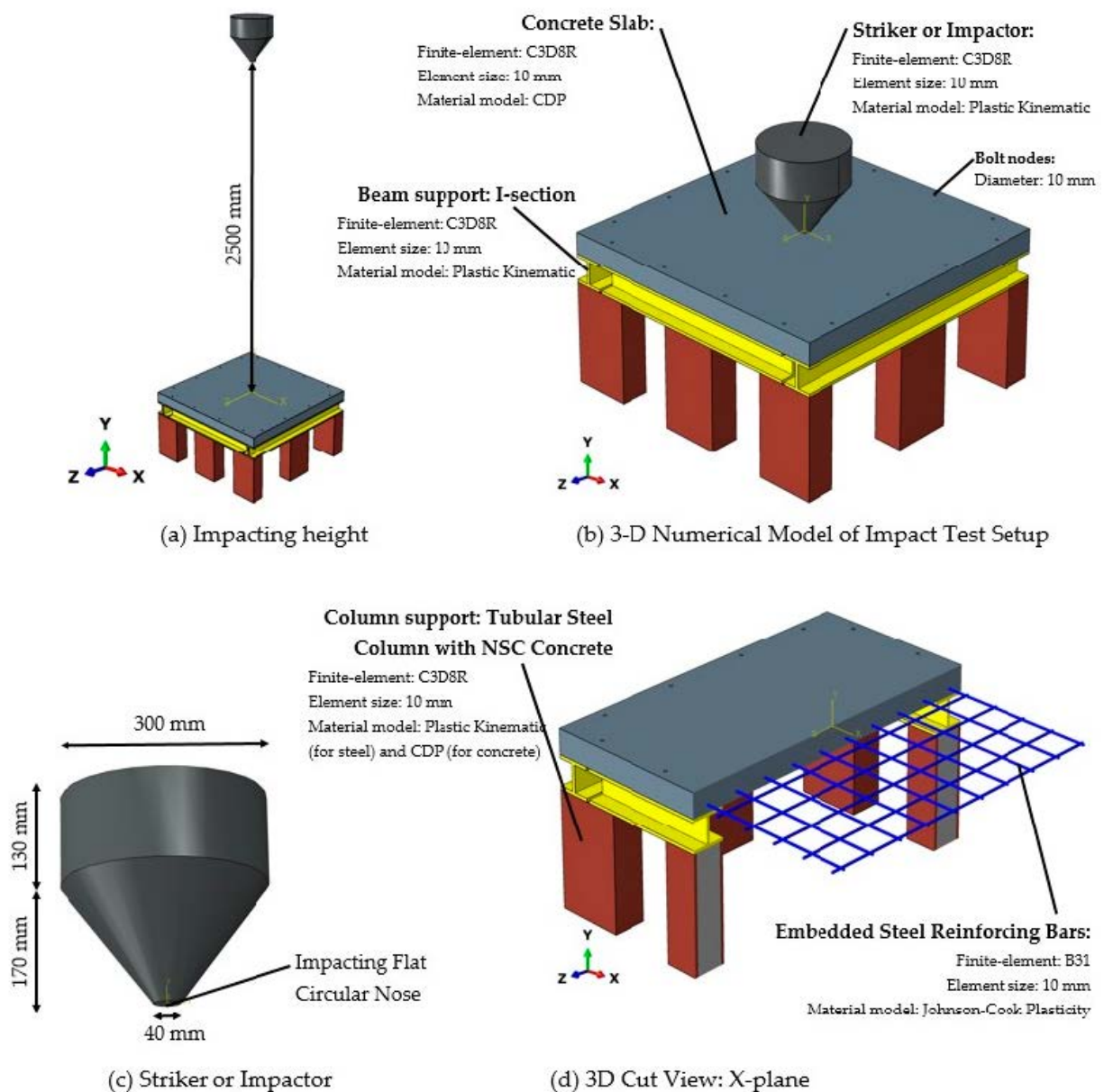


Figure 1. Detailed model of impact load test setup.

The CDP damage parameter, d , as discussed above, can also be related to damage dissipation energy (DDE) and total absorbed energy (Q), as follows [38]:

$$Q - D_{DE} = (1 - d)Q \quad (2)$$

$$d = \frac{D_{DE}}{Q} \quad (3)$$

DDE [38], a mechanical strain-based energy parameter, can be defined as the amount of energy dissipated by the damage due to the applied impulsive loading on the slab. In order to quantify the damage, this dissipated energy-related parameter is considered in the present work.

The striker is modeled as a rigid body considering its very high yield strength and limited deformation during simulations. The diameter of the impacting face of the striker is 40 mm. The constitutive model used for the steel bars is the Johnson–Cook plasticity model, while for the striker and supports, the model used is plastic kinematic.

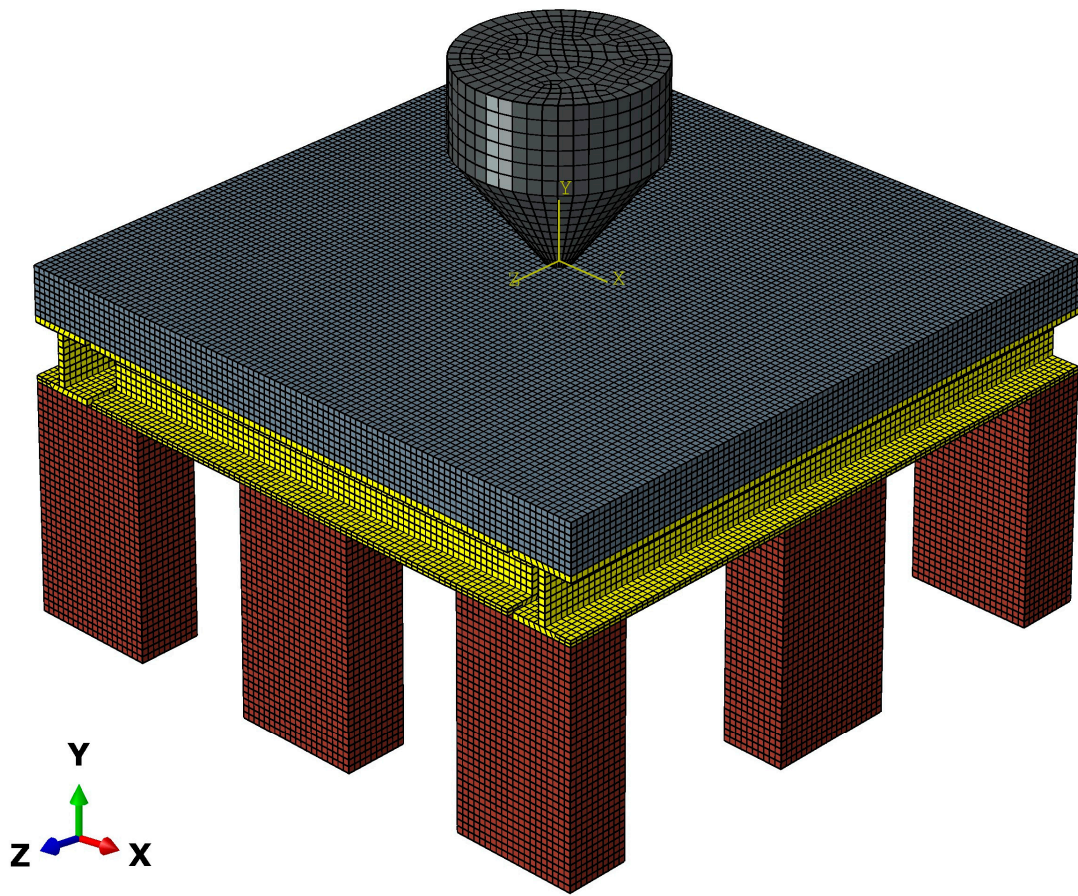


Figure 2. Finite element model.

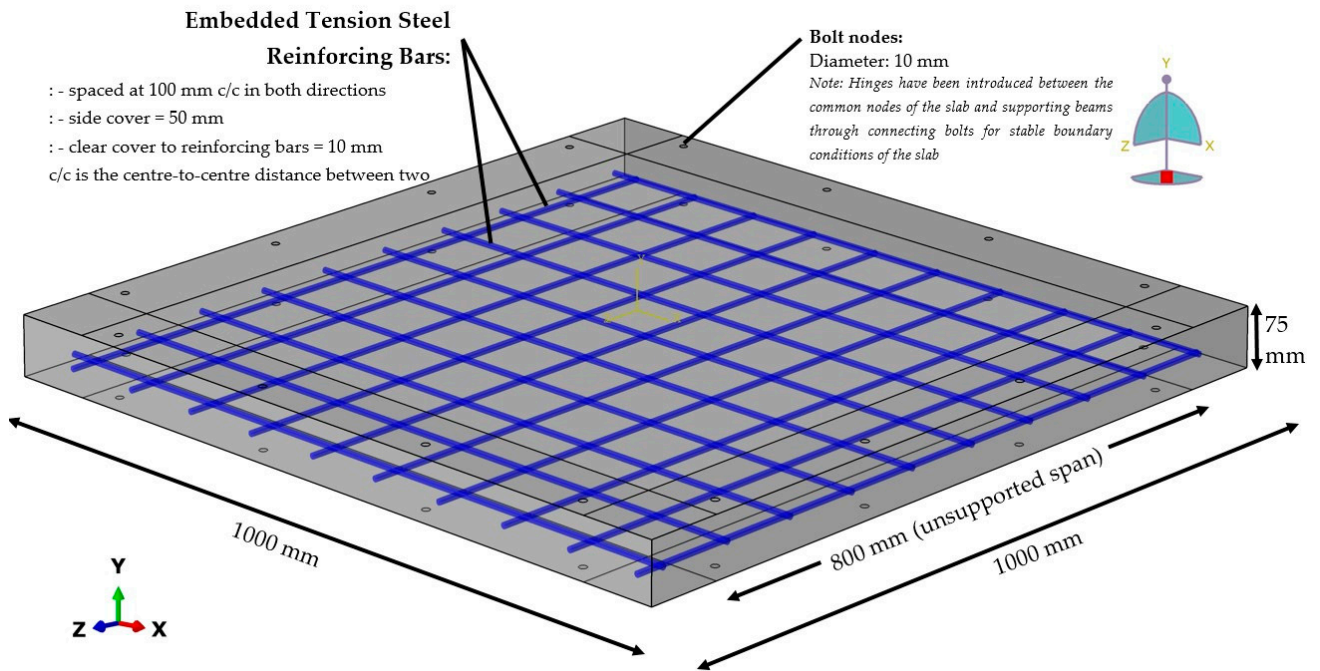


Figure 3. Rendered view of the embedded reinforcing tension steel bars.

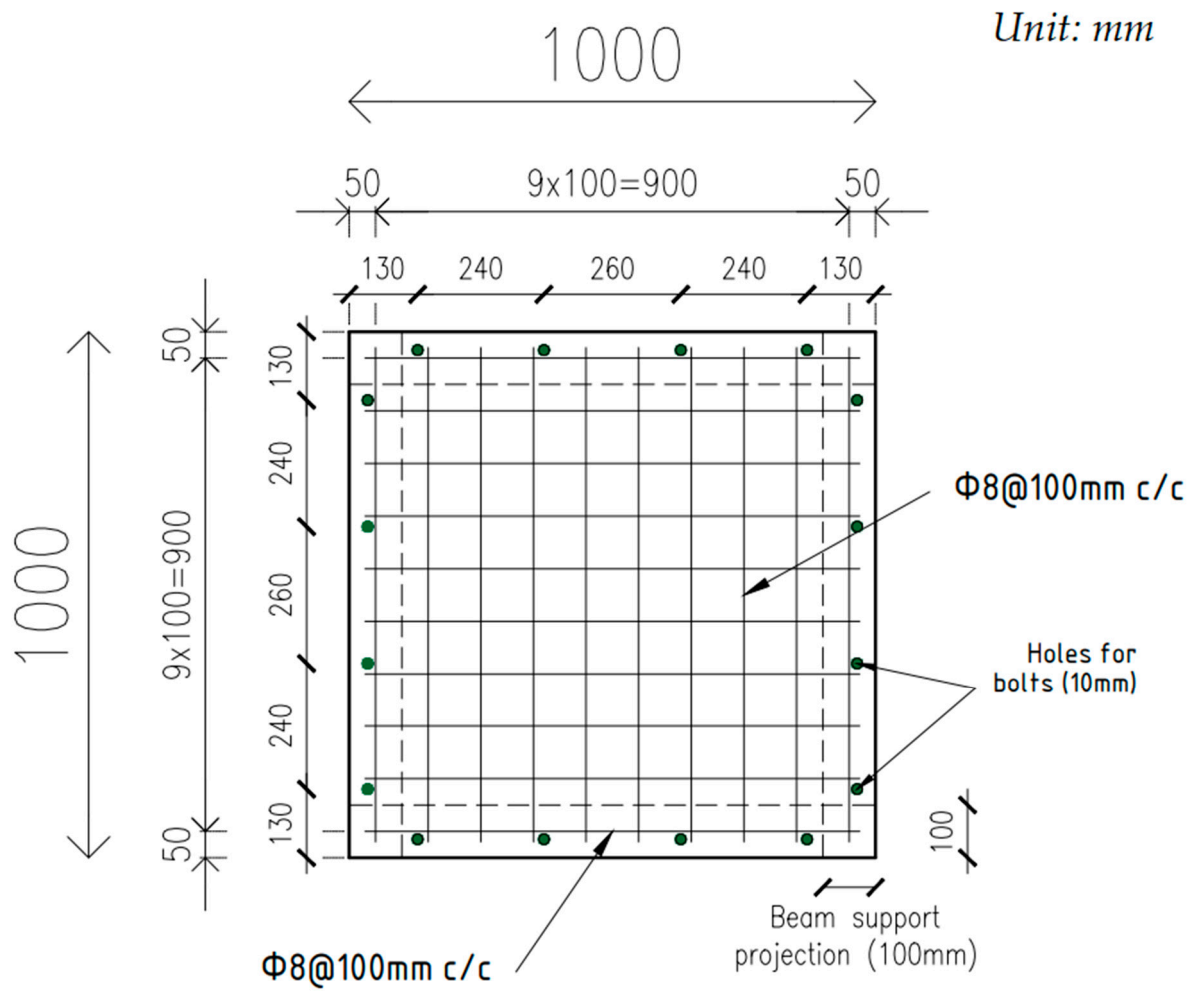
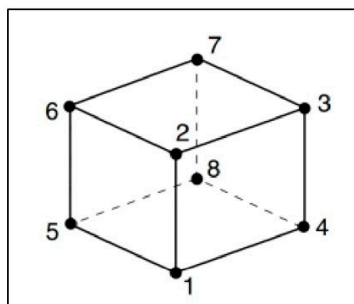
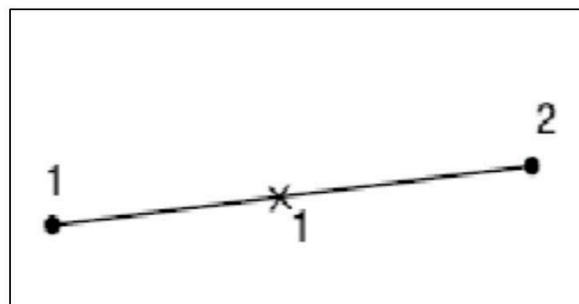


Figure 4. Reinforcement details of the slab.



(a) C3D8R



(b) B31 with one integration point

"B31" is a 2-node beam element with linear interpolation formulations in three-dimensional space.

"C3D8R" is an 8-node linear hexahedral solid element with reduced integration and hourglass control

Figure 5. Element shape of C3D8R and B31 finite elements considered in this study.

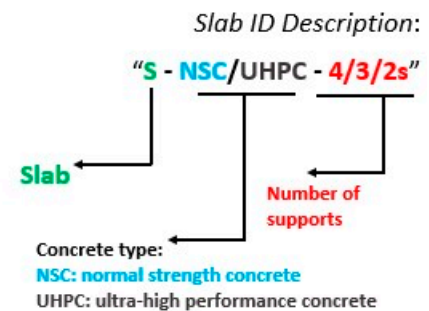
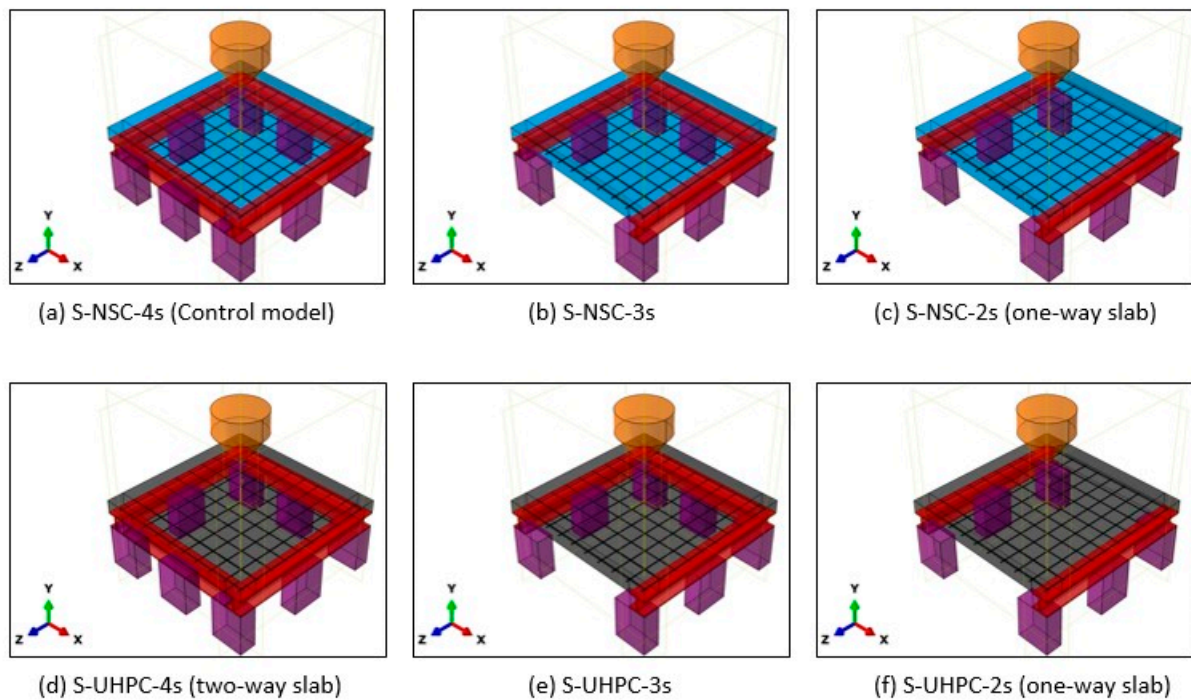


Figure 6. Slab models created in the ABAQUS software.

According to the current literature [2–4,13,44], the JCP model (formerly known as the Cook model) is most commonly used to define the behavior of steel material owing to its simplicity in comparison to other material models; the same has been employed for defining properties for reinforcing bars in this work. This model expresses Von Mises flow stress (often called equivalent shear stress, σ_{eq}) as a function of strain hardening, strain hardening/sensitivity rate, and thermal softening (temperature change) [13,38]. The following equation [38] represents a JCP model:

$$\sigma_{eq} = \left(A + B\varepsilon_{eq}^{pln} \right) \left[1 + C \ln \left(\frac{\dot{\varepsilon}}{\varepsilon_0} \right) \right] \left[1 - \left(\frac{T - T_0}{T_{melt} - T_0} \right)^m \right] \quad (4)$$

where $\left(A + B\varepsilon_{eq}^{pln} \right)$ accounts for strain hardening; $\left[1 + C \ln \left(\frac{\dot{\varepsilon}}{\varepsilon_0} \right) \right]$ = rate sensitivity effects; $\left[1 - \left(\frac{T - T_0}{T_{melt} - T_0} \right)^m \right]$ = temperature change effects; A , B , C , m , and n are material constants; ε_{eq}^{pl} represents equivalent plastic strain; $\dot{\varepsilon}$ and ε_0 are plastic and reference strain rates, respectively; T_0 = transition temperature; and T_{melt} represents a melting point of the material. Johnson–Cook parameter values are obtained from refs. [2,3,13]. A detailed description of these constitutive models is available in refs. [2,3,13]. Simple support boundary conditions are assigned to the slab, the same used by the authors of [2,3,13]. The connection between concrete and striker is defined using interaction keycards considering hard contact with

penalty contact formulation, as reported in [2,3,13]. Imposed acceleration, velocity, deflection, and material stress to the slab using the striker are all taken into account using this technique. The strength increase brought on by a rapid rate of strain is a major factor in the mechanical behavior of materials subjected to extreme loadings. Impact loading generates high-strain rates, typically between 10^2 and 10^3 s^{-1} (Figure 7) [1–3]. For instance, this phenomenon has a significant influence on structures made of reinforced concrete. Their resistance might rise significantly, with dynamic coefficients of 3 for compression and 6 for tension, as reported in [2,3,41,42]. Note that the dynamic coefficients used to incorporate strain-rate effects are briefly discussed in refs. [2,3]. The striker does not penetrate through the slab when the load is applied, and following contact, it remains apart. The impact load is applied using the command “initial_velocity_generation” [2,3,38]. The concrete–steel reinforcement connection is defined using the constraint “embedded region” [2,3]. Altogether, five face-to-face interaction contacts [2,3,38] are used in the modeling: striker–concrete, striker–steel bars, steel bars–concrete, slab–steel beams, and beams–columns. Moreover, static and dynamic coefficients of friction considered are 0.20 and 0.10, respectively. Note that the striker can only cause translation in the global Y-direction (impact direction) while the X- and Y-translations as well as X-, Y-, and Z-rotations are all restricted. The nonreflecting constraint is imposed all around the slab model.

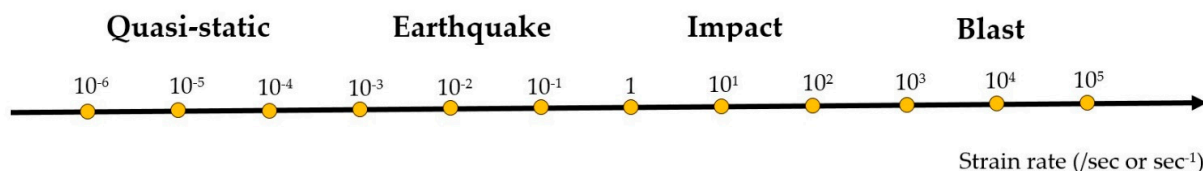


Figure 7. Different structural loadings and corresponding strain rate ranges.

2.3. Material Properties

Two different kinds of concrete are used in the simulation presented herein: (1) normal-strength (NSC) and (2) ultra-high performance (UHPC). The static compressive strengths of NSC and UHPC are 29.70 MPa [13] and 99.50 MPa, respectively. The values of the elastic moduli of the concretes used are 30.91 GPa [13] and 51 GPa, respectively. The static yield strength and modulus of elasticity of steel bars are 422 MPa and 198 GPa, respectively [13]. Poisson’s ratio of 0.20 for concrete and 0.30 for steel is considered. Other material properties of the impact test setup are briefly described in refs. [2,3,13]. The data collected by the authors of [2,3,13] for NSC and by the authors of [38] for UHPC are utilized in defining the plastic response of the concrete material. The calibrated compressive and tensile behaviors of NSC and UHPC are shown in Figures 8A and 8B, respectively. The original CDP properties of concrete are available in ref. [38]. Both softening and hardening behaviors are considered in the simulations following this reference only. It can be seen from Figure 8 that the calibrated strengths (i.e., dynamic strengths) are much higher compared to the abovementioned static strengths on account of loading rate or dynamic strength effects, which are necessary to be taken into account while conducting numerical analysis under high strain-rate or extreme loadings induced by impact or blast. Following the current literature [2,3,41–45], the strain-rate effects are incorporated into the modeling by considering dynamic increase factors (DIFs) (often called stress-increase factors) which are assumed constant. Note that this procedure is not fully objective; however, many researchers have followed the same methodology in their validation of the numerical or finite element models under such extreme loading conditions, as reported in refs. [43–45]. The calibrated dynamic strengths are shown in Figure 8. For reinforcing steel, a DIF of 1.25 is considered, following UFC 3-340-02 (2008) [42].

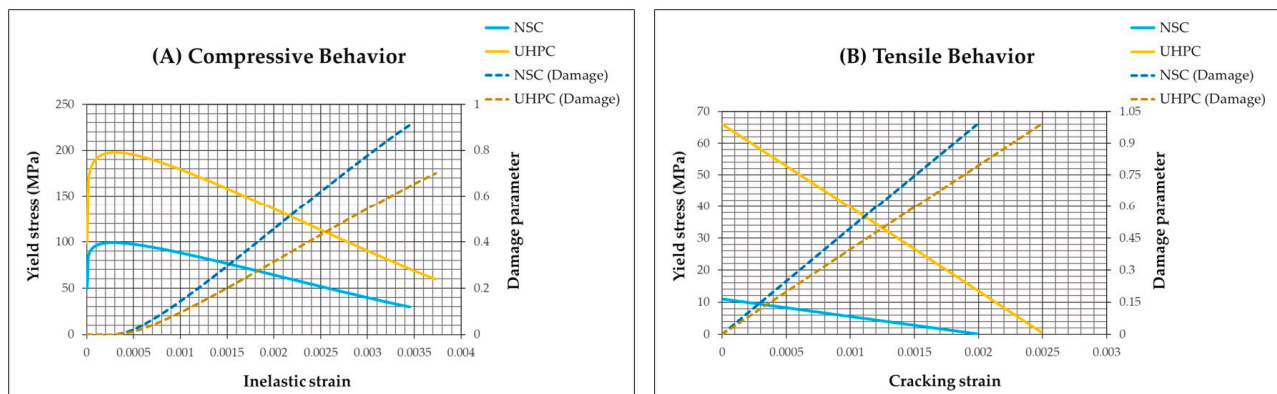


Figure 8. CDP compressive and tensile behaviors for NSC and UHPC materials.

2.4. Application of Impact Load on Slab Top Face

During the impact simulations, the energy and mass loss effects of the striker are neglected in this study to allow its potential energy to be solely transformed into kinetic energy, and it is simple to determine the free-fall velocity of the impact as $V_0 = \sqrt{2gH}$, g = gravity ($=9805 \text{ mm/s}^2$) and H = impact height (in this case = 2500 mm) [2,3,13]. Note that the load is applied to the centroid of the slab using the explicit module of the software considering $V_0 = 7.0 \text{ m/s}$, free-fall time of 0.71 s [2,3], and a total impact duration of 1.0 s. The applied energy to the impacting face of the slab can be calculated using Equation (5), [13]:

$$E = NmgH \quad (5)$$

where N = number of impacts; m = striker mass. In this case, $N = 1$, $m = 105 \text{ kg}$, $g = 9805 \text{ mm/s}^2$, and $H = 2500 \text{ mm}$.

2.5. Mesh-Sensitivity Analysis

An essential characteristic to take into account in the computational problems related to high-rate dynamic simulations is mesh density, which has a significant impact on the outcomes of the analysis [2,3,44]. To optimize the element sizes for even more exact results and to reduce the necessary computing time, a mesh sensitivity analysis is done in this respect [2,3]. Finite element sizes of 10, 15, and 20 mm for the slab are considered. The influence of increasing the element size on the displacement as well as damage to the slab is considered, and the computed outcomes are compared with the experimental ones reported in ref. [13]. The discrepancies between the experimental findings and the modeling results are shown in Figures 9 and 10. These figures show that the simulation findings with a 10 mm size are reasonably close to the experimental results. The experimentally recorded and numerically simulated displacement-time curves with this size are almost identical. However, it is noted that the test findings and the analysis results show some discrepancies. This could be a result of the limitations and idealizations involved in the material modeling as well as in the support conditions that were used.

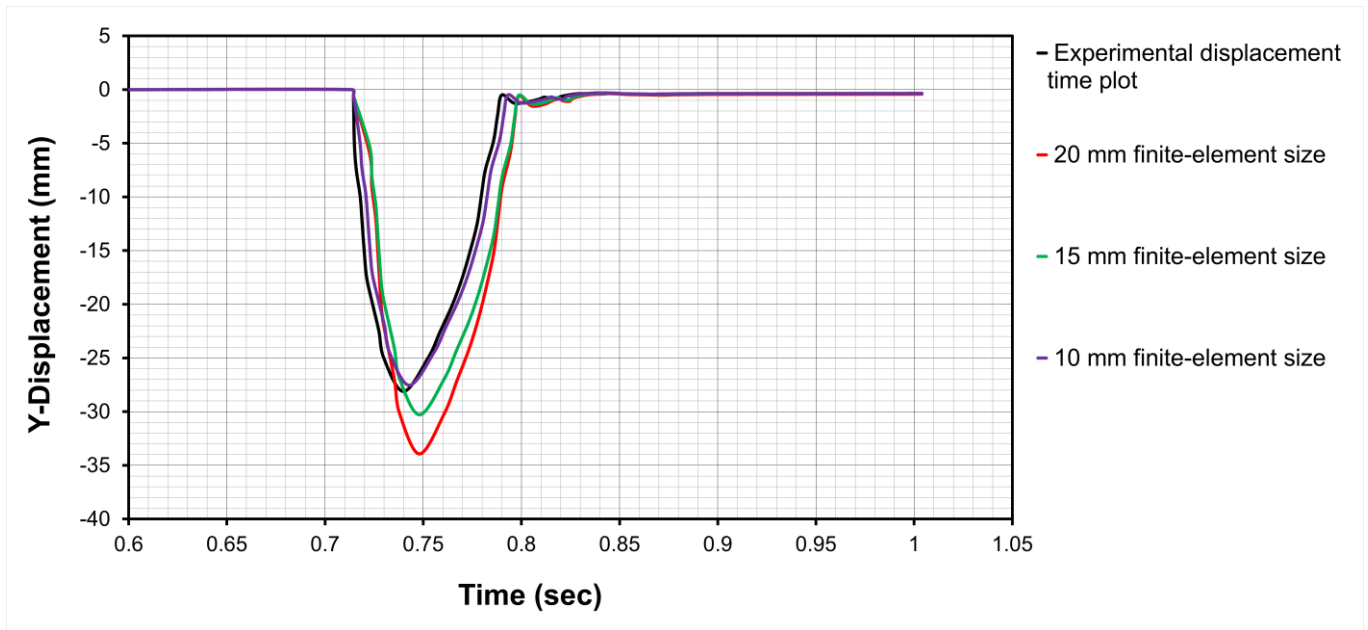
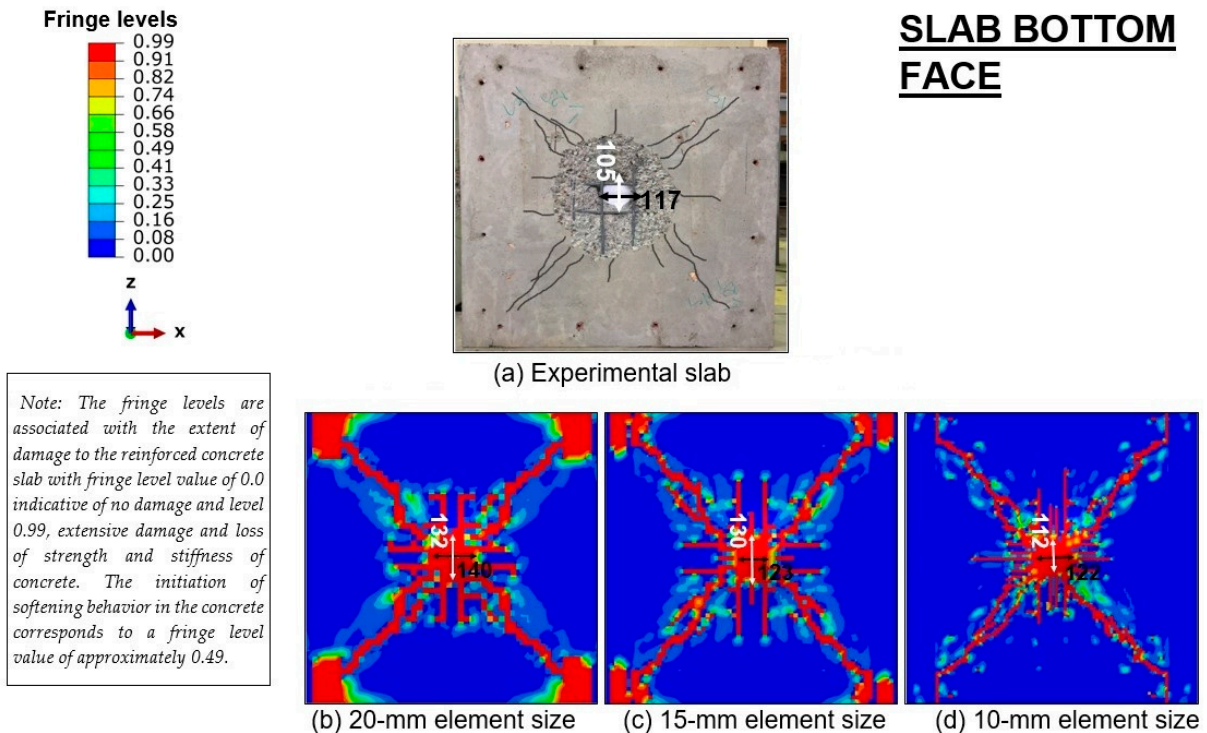


Figure 9. Comparison between experimental and numerical results: displacement time plots.



Unit: mm

Figure 10. Comparison between experimental and numerical results: damage profiles.

3. Results and Discussion

Images taken from the impact simulation analyses are shown in Figures 11–16. Response parameters considered in this work are: (1) damage profiles, (2) vertical displacement, (3) principal stresses, (4) equivalent plastic strain, and (5) damage dissipation energy (DDE). The moment the dropping mass impinges on the slab top surface, fragments of the concrete from the immediate vicinity of the impacted area eject along with the punching of the slab concrete (Figures 11 and 12). On the counterpart slab surface, bond failure occurs in

the neighboring flexural zone of the impacted area and major diagonal cracks develop from the punching shear plane, Figure 11. The distribution of the vertical displacement in the slab and its embedded reinforcing steel is shown in Figure 13; the control slab experiences a maximum displacement of 27.31 mm in the Y-direction at the impacted region, while the other two slabs, namely S-NSC-3s and S-NSC-2s, display slight higher peak displacements of 33.96 mm and 34.82 mm, respectively, as compared to the control model or slab. Both primary and secondary reinforcing bars at the impacted area or region of the control slab experience a peak displacement of 21.27 mm in the Y-direction, as shown in Figure 13. The bars of slabs S-NSC-3s and S-NSC-2s deform in the direction of applied impact and show maximum displacements of 27.03 mm and 29.22 mm, respectively. Maximum principal stresses (compressive: -ve; and tensile: +ve) in the reinforcing steel of the considered slabs are represented in Figure 14. Note that the stress level at most of the locations for slabs made of NSC concrete exceeds the yield stress level (422 MPa) of the steel. However, the stress response of the steel bars is improved with the use of UHPC in lieu of NSC in the slabs, as shown in Figure 14. UHPC slabs shown in Figure 15 display a similar trend of the displacements as those of the NSC slabs. Equivalent plastic strains (PEEQ) in the slabs, estimated with ABAQUS built-in CDP and Johnson–Cook properties, are shown in Figure 16. The concrete at the impacted region of the control or reference slab (S-NSC-4s) experiences a maximum plastic strain of 0.14, which is slightly higher than the plastic strains in the slabs S-NSC-3s and S-NSC-2s (see Figure 16) on account of the change of the mode of failure and the uplifting of corners of the free edge(s) of these slabs, as discussed as follows.

The propagation of the bond failure is more pronounced toward the free edge than toward the three restrained edges of the slab S-NSC-3s (Figure 11). In this slab, the damage to the bond in the flexural zone around the shearing plane is more toward the free edge as compared to restrained edges. For some of these bars perpendicular to the free edge, the damage to the bond is continuous but partial. This slab undergoes peak displacement in the Y-direction of 32.23 mm at the impacted region, which is more than the displacement of the control model (27.31 mm). Although diagonal cracks do originate from the shearing plane and propagate toward the corners (A and B) consisting of one free edge, they are not much less severe than the other two diagonal cracks toward the corners (C and D) consisting of restrained edges. The severity of the diagonal cracks increases toward the restrained corners C and D, while decreases toward the corners A and B. Corners A and B tend to lift up and become damaged, while the other two corners C and D are not damaged at all. Consequently, the slab supported on three edges suffers more damage (DDE = 205.38 J) and undergoes higher maximum displacement (32.23 mm) than the control slab supported on four edges (Table 1 and Figure 13).

Table 1. Simulation results.

S. No.	Specimen	* Δ_y (mm)		DDE (J)	α_y (g)	S_t (MPa)
		Slab	Bars			
1	S-NSC-4s	−27.31	−21.27	190.97	294.72	426.39
2	S-NSC-3s	−33.96	−27.03	209.57	135.07	479.94
3	S-NSC-2s	−34.82	−29.22	204.88	129.26	525.22
4	S-UHPC-4s	−4.39	−3.85	92.76	395.15	421.56
5	S-UHPC-3s	−5.27	−5.0	104.78	197.77	427.0
6	S-UHPC-2s	−8.49	−7.93	98.12	189.61	466.24

* Δ_y = Max^m displacement in Y-direction at the point of impact; DDE = damage dissipation energy; α_y = peak acceleration in Y-direction; S_t = Max^m tensile stress in the steel bars at the point of impact; g = acceleration due to gravity.

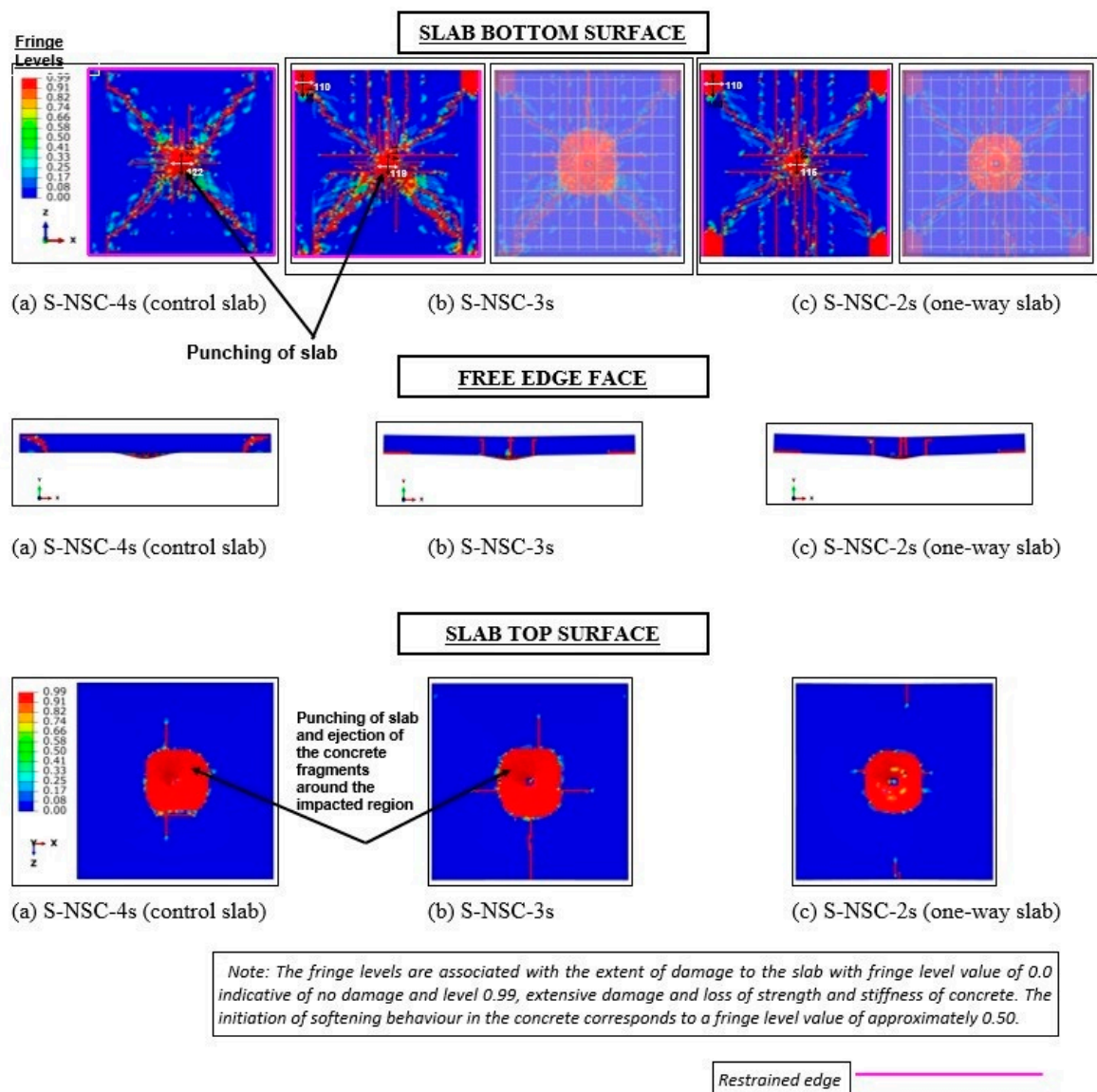


Figure 11. Damage to the NSC slabs by applied impact load at $t = 0.735$ s, the time at which the slab attains maximum displacement.

The slab supported on two opposite edges, i.e., one-way slab S-NSC-2s, has four identical corners. Under impact loading, the stress waves propagate in all four directions, which cause them to transfer the load both ways, thereby generating diagonal cracks from the punching shear plane toward the corners (Figure 11). Main re-bars experience much higher tensile stress ($525.22 \text{ MPa} > \text{yield stress} = 422 \text{ MPa}$) than distribution re-bars (480.84 MPa) (Figure 14). The spread of the maximum stress is much more in the re-bars under the impacted area than in the adjacent main re-bars. It is noted that maximum tensile stress in the main bars passing through the impacted or punching area is witnessed by de-bonding beyond the shearing plane in the flexure zone. This spread gradually decreases toward the free edges of the slab (Figure 15). Along the width, flexural cracks through the shearing area develop due to the yielding of main bars. Corners consisting of one free edge experience identical damage in the form of concrete detachment at the bottom face of thickness equal to cover concrete (10 mm) due to their torsional uplifting. This slab experiences a maximum vertical downward displacement of 34.82 mm, which is much more than the displacement of the slab supported on four edges (27.31 mm), as well as the slab supported on three edges (33.96 mm) (Table 1). Note that the free edge of slab S-NSC-3s

undergoes a maximum downward displacement of 7.49 mm, while free edges of one-way slab S-NSC-2s experience an identical maximum downward displacement of 13.24 mm at the mid-span section (Figure 13 From Table 1), and the total damage in terms of DDE to the slab supported on two opposite edges (S-NSC-2s) is comparable to the slab supported on three edges (S-NSC-3s). However, the damage to the slab S-NSC-2s is only slightly lesser than the damage to the slab S-NSC-3s on account of wider and deeper diagonal cracks in the slab S-NSC-3s. The average depth of diagonal cracks all along their lengths is found to be 65 mm, while the depth of flexural cracks along the mid-span section is 75 mm. Damage to a corner of slab S-NSC-3s is found to be identical to the damage to a corner of slab S-NSC-2s. Thus, slab S-NSC-2s at its corner experiences double the damage at the corners of slab S-NSC-3s. The formation of slightly deeper and parallel diagonal cracks in slab S-NSC-3s indicates that dissipated damage energy on account of the development of these diagonal cracks is higher than in slab S-NSC-2s.

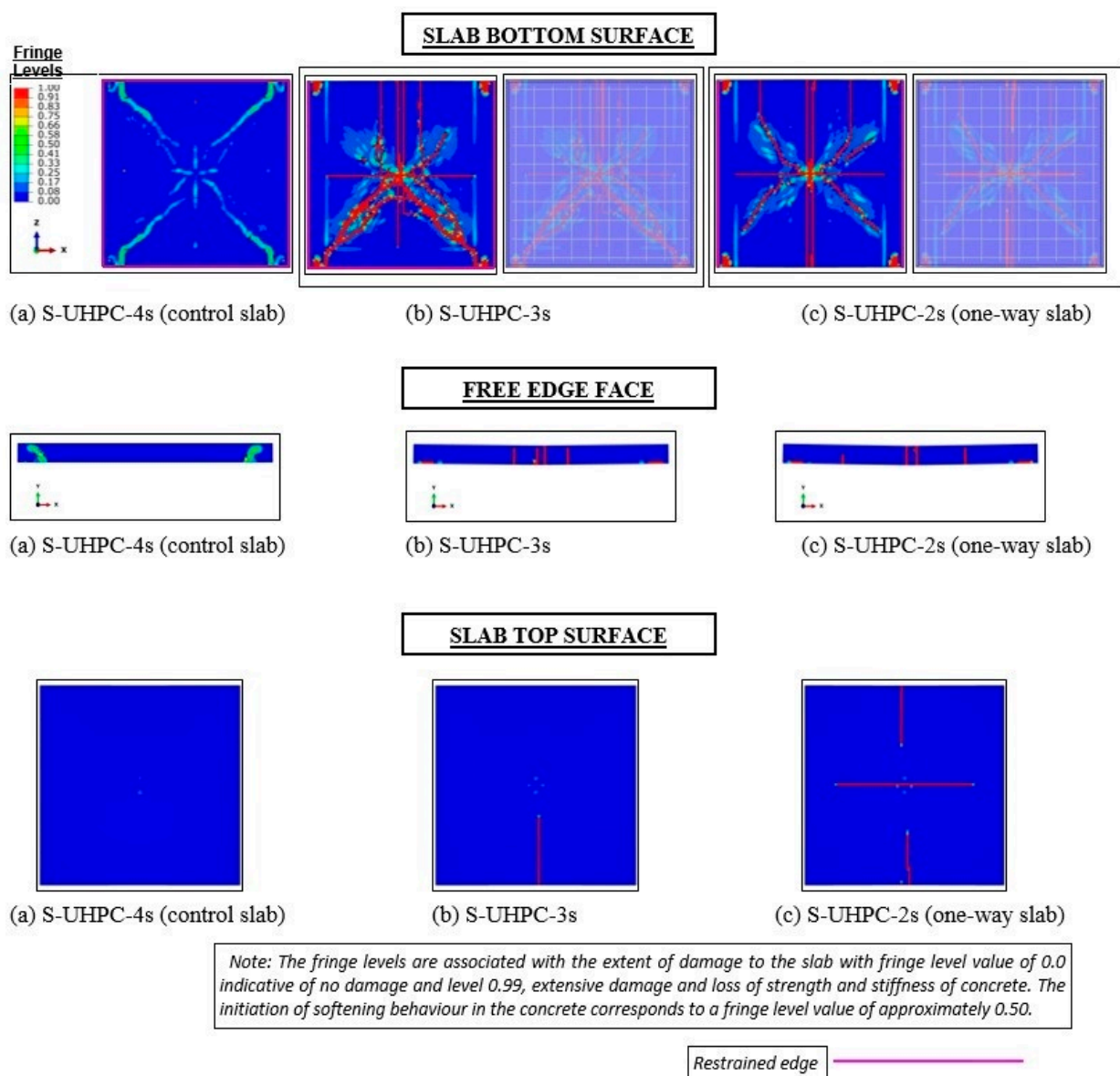
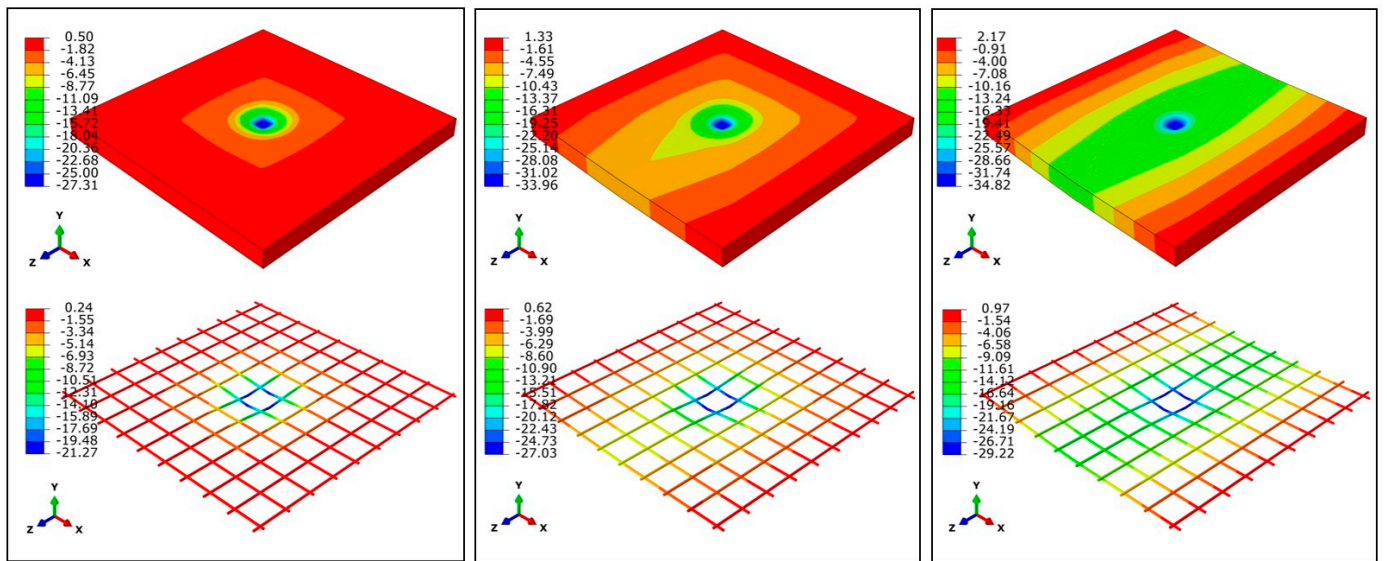


Figure 12. Damage to the UHPC slabs by applied impact load at $t = 0.735$ s.



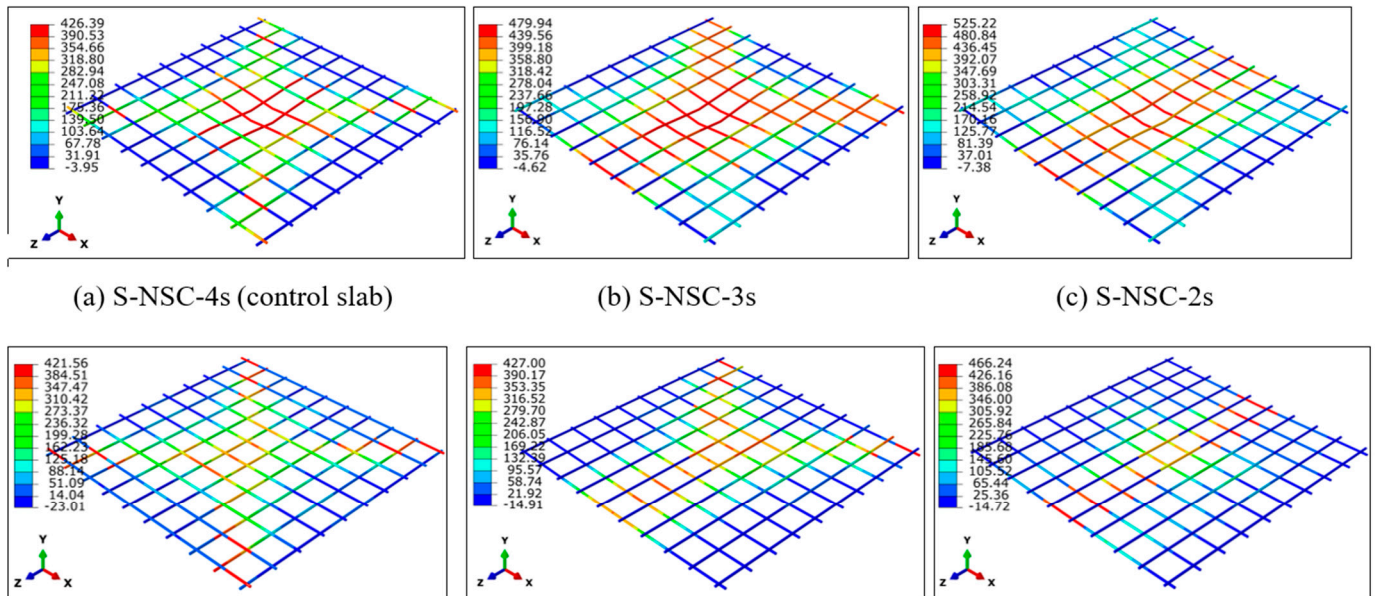
(a) S-NSC-4s (control slab)

(b) S-NSC-3s

(c) S-NSC-2s

Unit: mm

Figure 13. Y-displacement of NSC slabs at $t = 0.735$ s.



(a) S-NSC-4s (control slab)

(b) S-NSC-3s

(c) S-NSC-2s

(d) S-UHPC-4s

(e) S-UHPC-3s

(f) S-UHPC-2s

Unit: MPa
Note: +ve values indicate tensile

Figure 14. Principal stress contour of the embedded steel of the slabs at $t = 0.735$ s.

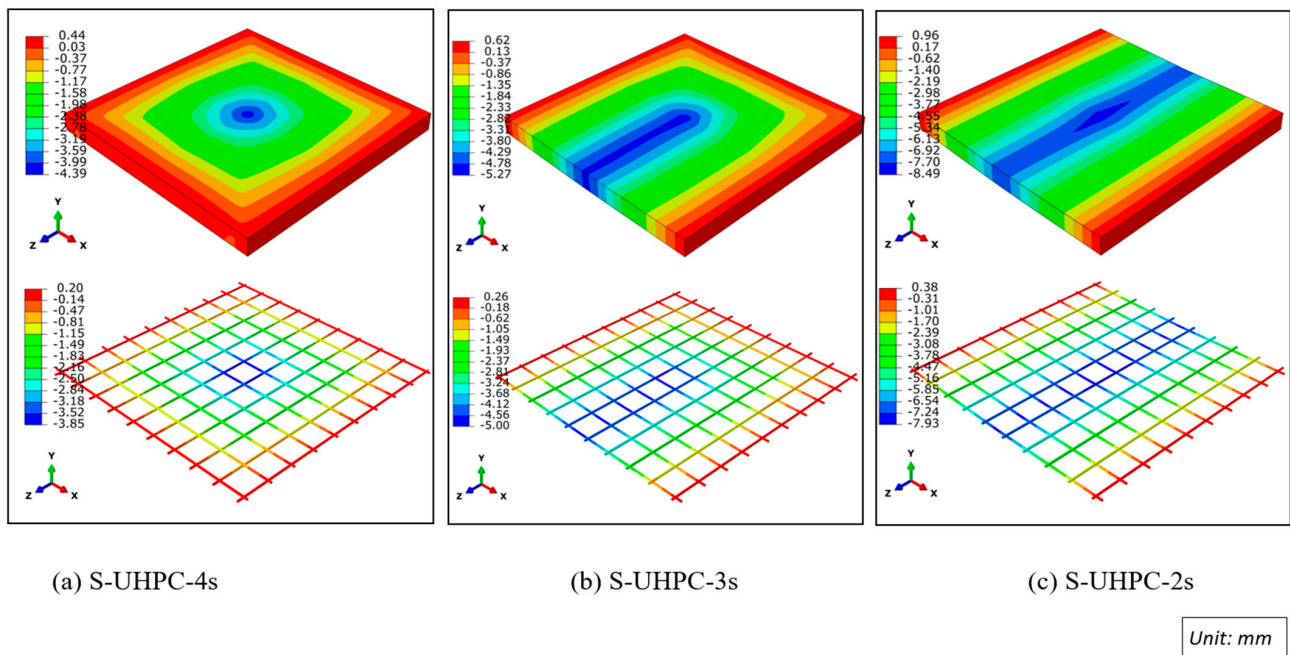


Figure 15. Y-displacement of UHPC slabs at $t = 0.735$ s.

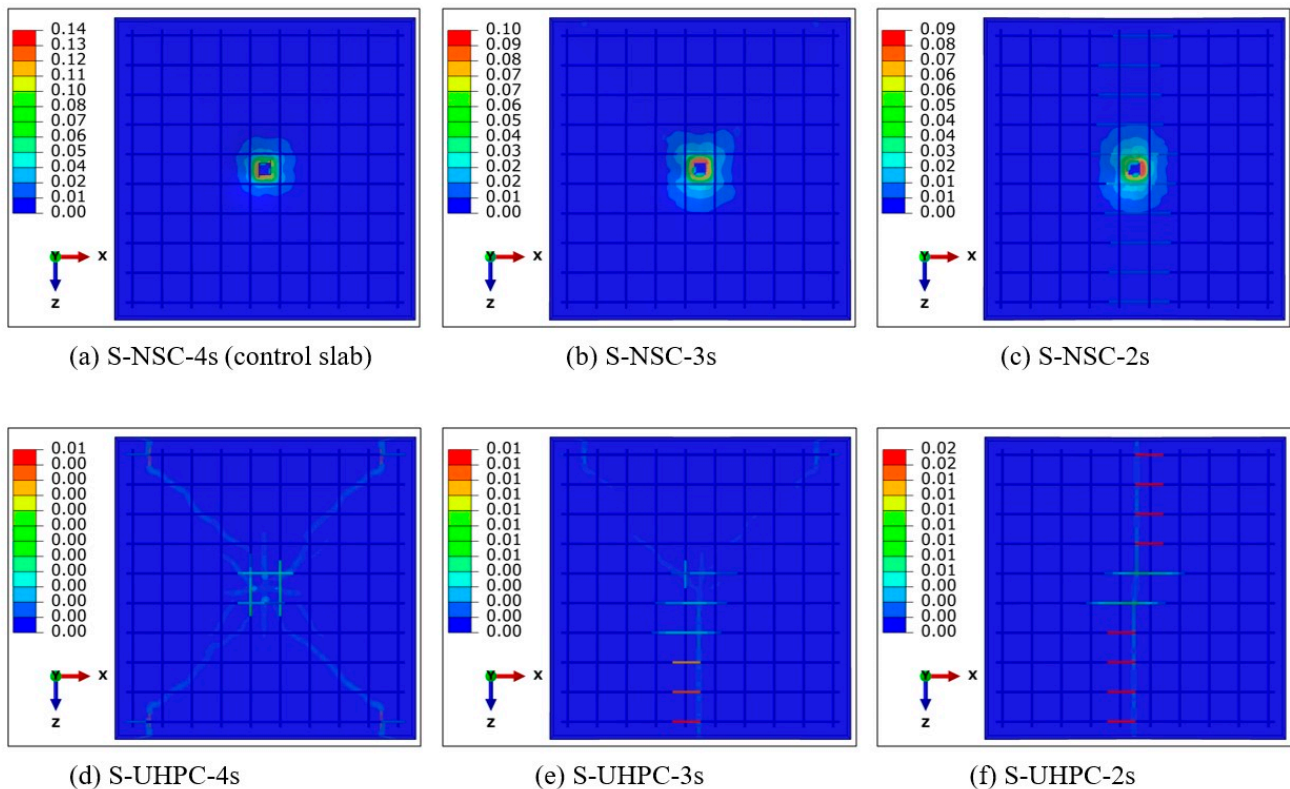


Figure 16. Equivalent plastic strain distribution on the top surface of the NSC and UHPC slabs at $t = 0.735$ s.

Data shown in Table 1 reveal that the peak acceleration of the slab is governed by its stiffness under impact. Increasing the compressive strength of concrete from 29.71 MPa (NSC) to 99.50 MPa (UHPC) in the slab S-UHPC-4s supported on all four edges, the displacement of the slab is reduced from 27.31 mm (in slab S-NSC-4s) to 4.39 mm (see Figure 15) without punching, and the dissipated energy by damage is de-

creased from 190.97 J to 92.76 J with nominal diagonal cracks of depth 12 mm. Results with regard to displacement, acceleration, DDE, and stresses in the reinforcing steel of the slabs with UHPC follow a similar trend, followed by the slabs with NSC (Table 1). Maximum displacement at the impacted area and total damage energy ratios of NSC slab/UHPC slab are given in Table 2.

Table 2. Displacement and damage ratios of NSC slab/UHPC slab under the drop weight.

Slab Supported On	Maximum Displacement Ratio	Damage (DDE) Ratio	Remark
Four edges (4s)	1:0.160	1:0.485	UHPC slabs respond (1) identically in the case of 4s and 3s models with regard to displacement and damage; (2) more contributes to control displacement than damage for the 2s model.
Three edges (3s)	1:0.155	1:0.499	
Two opposite edges (2s)	1:0.243	1:0.478	

4. Conclusions

This work presents the investigation carried out on the effect of supports and the role of UHPC on the dynamic response of square reinforced concrete slab, with only tension steel reinforcement subjected to low-velocity drop load. The slabs are: supported on all four edges (S-NSC/UHPC-4s), supported on three edges (S-NSC/UHPC-3s), and supported only on two opposite edges (S-NSC/UHPC-2s) with NSC and UHPC concretes.

Major findings are:

- Simulation results show that the total energy dissipated through the damage of the slab supported on three edges is greater than that of the slab supported on all four edges, as well as the slab supported only on two opposite edges on account of the formation of a higher number of wider and deeper diagonal cracks and severe punching.
- Domination of the flexure in the slab S-NSC/UHPC-2s indicated by maximum tensile stress in the steel re-bars supplemented by their maximum displacement under the impacted area shows that damage due to shearing of concrete in this slab is less than that of the slab S-NSC/UHPC-3s. This is why the damage to the slab S-NSC/UHPC-3s is maximum.
- Damage in the form of the detachment of cover concrete at the corners consisting of free edge(s) of the slabs S-NSC/UHPC-3s and S-NSC/UHPC-2s occurs due to impulsive reaction at such corners, which makes the steel bars exposed. These slabs undergo severe diagonal cracking and de-bonding in the flexure zone as compared to the slab S-NSC/UHPC-4s.
- The depth of the diagonal cracks toward the restrained corners of slab S-NSC/UHPC-3s is a little higher than that of diagonal cracks toward the corners having one free edge. This shows that the supports' effects have a significant influence on the dynamic response and failure mode of the RC slab under impact loading.
- UHPC replaced for NSC in the slabs with similar supports greatly improves the impact response and follows a similar trend of results as those of the slabs with NSC. UHPC slabs show identical behavior for 4s and 3s models with regard to maximum displacement and damage, while for the 2s model, it contributes more to control the displacement than damage.

Author Contributions: Conceptualization, S.M.A., M.S., M.A. (Mehtab Alam) and A.M.Y.; methodology, S.M.A. and M.A. (Mehtab Alam); software, S.M.A., M.S., A.M.Y. and M.A. (Mohamed AbdelMongy); validation, S.M.A., M.S., A.M.Y., A.M. and M.A. (Mohamed AbdelMongy); formal analysis, M.S., A.M.Y. and A.M.; investigation, S.M.A.; resources, M.S., A.M.Y. and A.M.; data curation, S.M.A. and M.A. (Mohamed AbdelMongy); writing—original draft preparation, S.M.A., M.S., M.A. (Mehtab Alam), A.M.Y., A.M. and M.A. (Mohamed AbdelMongy); writing—review and editing, M.A. (Mehtab Alam) and M.A. (Mohamed AbdelMongy); visualization, M.A. (Mehtab Alam) and M.A. (Mohamed AbdelMongy); supervision. All authors have read and agreed to the published version of the manuscript.

Funding: This research received no funding.

Institutional Review Board Statement: Not applicable.

Informed Consent Statement: Not applicable.

Data Availability Statement: Not applicable.

Acknowledgments: Previous experimental, numerical, and analytical studies performed by the eminent Professor Hong Hao from the Department of Civil and Construction Engineering, Curtin University, Bentley (Western Australia) provide the authors with great motivation to work in this field of research. The studies also help the authors in understanding the modeling of impact loading, load-carrying mechanism, and modeling of structural response to extreme loads. The authors are very fortunate and grateful to have inspiration from Hong Hao and deeply thank him.

Conflicts of Interest: The authors declare no conflict of interest. The funders had no role in the design of the study; in the collection, analyses, or interpretation of data; in the writing of the manuscript; or in the decision to publish the results.

References

1. Abbas, H.; Gupta, K.N.; Alam, M. Nonlinear response of concrete beams and plates under impact loading. *Int. J. Impact Eng.* **2004**, *30*, 1039–1053. [[CrossRef](#)]
2. Anas, S.M.; Alam, M.; Shariq, M. Behavior of two-way RC slab with different reinforcement orientation layouts of tension steel under drop load impact. *Mater. Today Proc.* **2022**, *in press*. [[CrossRef](#)]
3. Anas, S.M.; Alam, M. Role of shear reinforcements on the punching shear resistance of two-way RC slab subjected to impact loading. *Mater. Today Proc.* **2022**, *in press*. [[CrossRef](#)]
4. Ozgür, A.; Kantar, E.; Yilmaz, M.C. Low velocity impact behavior of RC slabs with different support types. *Constr. Build. Mater.* **2015**, *93*, 1078–1088.
5. Kumar, V.; Iqbal, M.A.; Mittal, A.K. Impact resistance of prestressed and reinforced concrete slabs under falling weight indenter. *Procedia Struct. Integr.* **2017**, *6*, 95–100. [[CrossRef](#)]
6. Li, Y.; Chen, Z.; Ren, X.; Tao, R.; Gao, R.; Fang, D. Experimental and numerical study on damage mode of RC slabs under combined blast and fragment loading. *Int. J. Impact Eng.* **2020**, *142*, 103579. [[CrossRef](#)]
7. Yao, S.; Zhang, D.; Chen, X.; Lu, F.; Wang, W. Experimental and numerical study on the dynamic response of RC slabs under blast loading. *Eng. Fail. Anal.* **2016**, *66*, 120–129. [[CrossRef](#)]
8. Wang, R.; Han, L.H.; Tao, Z. Behavior of FRP-concrete-steel double skin tubular members under lateral impact: Experimental study. *Thin-Walled Struct.* **2015**, *95*, 363–373. [[CrossRef](#)]
9. Sha, Y.; Hao, H. Laboratory tests and numerical simulations of CFRP strengthened RC pier subjected to barge impact load. *Int. J. Struct. Stab. Dyn.* **2015**, *15*, 1–33. [[CrossRef](#)]
10. Soltani, H.; Khaloo, A.; Sadraie, H. Dynamic performance enhancement of RC slabs by steel fibers vs. externally bonded GFRP sheets under impact loading. *Eng. Struct.* **2020**, *213*, 110539. [[CrossRef](#)]
11. Daneshvar, K.; Moradi, M.J.; Ahmadi, K.; Hajiloo, H. Strengthening of corroded reinforced concrete slabs under multi-impact loading: Experimental results and numerical analysis. *Constr. Build. Mater.* **2021**, *284*, 122650. [[CrossRef](#)]
12. Colombo, M.; Martinelli, P.; Arano, A.; Øverli, J.A.; Hendriks, M.A.; Kanstad, T.; di Prisco, M. Experimental investigation on the structural response of RC slabs subjected to combined fire and blast. *Structures* **2021**, *31*, 1017–1030. [[CrossRef](#)]
13. Sadraie, H.; Khaloo, A.; Soltani, H. Dynamic performance of concrete slabs reinforced with steel and GFRP bars under impact loading. *Eng. Struct.* **2019**, *191*, 62–81. [[CrossRef](#)]
14. Zineddin, M.; Krauthammer, T. Dynamic response and behavior of reinforced concrete slabs under impact loading. *Int. J. Impact Eng.* **2007**, *34*, 1517–1534. [[CrossRef](#)]
15. Mougin, J.P.; Perrotin, P.; Mommessin, M.; Tonnelo, J.; Agbossou, A. Rock fall impact on reinforced concrete slab: An experimental approach. *Int. J. Impact Eng.* **2005**, *31*, 169–183. [[CrossRef](#)]
16. Kishi, N.; Mikami, H.; Matsuoaka, K.G.; Ando, T. Impact behavior of shear-failure-type RC beams without shear rebar. *Int. J. Impact Eng.* **2002**, *27*, 955–968. [[CrossRef](#)]
17. Yılmaz, T.; Kırac, N.; Anil, Ö.; Erdem, R.T.; Sezer, C. Low-velocity impact behaviour of two way RC slab strengthening with CFRP strips. *Constr. Build. Mater.* **2018**, *186*, 1046–1063. [[CrossRef](#)]
18. Tahmasebinia, F.; Remennikov, A. Simulation of the reinforced concrete slabs under impact loading. *Australas. Struct. Eng. Conf. (ASEC)* **2008**, *10*, 26–27.
19. Tahmasebinia, F. Numerical Modeling of Reinforced Concrete Slabs Subjected to Impact Loads. Master's Thesis, Department of Civil Engineering, University of Wollongong, Sydney, Australia, 2008.
20. Saatci, S.; Vecchio, F. Nonlinear finite element modeling of reinforced concrete structures under impact loads. *ACI Struct. J.* **2009**, *106*, 717–725.

21. Ozbolt, J.; Sharma, A. Numerical simulation of reinforced concrete beams with different shear reinforcements under dynamic impact loads. *Int. J. Impact Eng.* **2011**, *38*, 940–950. [[CrossRef](#)]
22. Lee, J.Y.; Kim, M.H.; Min, K.H. Yoon, Y.S. Analysis of behaviors of concrete strengthened with FRP sheets and steel fibers under low-velocity impact loading. *J. Korea Inst. Struct. Maint. Insp.* **2011**, *15*, 155–164.
23. Lee, J.Y.; Shin, H.O.; Min, K.H. Yoon, Y.S. Analytical evaluation of high velocity impact resistance of two-way RC slab reinforced with steel fiber and FRP sheet. *J. Korea Inst. Struct. Maint. Insp.* **2013**, *17*, 1–9.
24. Zhao, W.; Qian, J. Dynamic response and shear demand of reinforced concrete beams subjected to impact loading. *Int. J. Struct. Stab. Dyn.* **2019**, *15*, 159–167. [[CrossRef](#)]
25. Wang, Y.; Qian, X.; Liew, J.Y.R.; Zhang, M.H. Impact of cement composite filled steel tubes: An experimental, numerical and theoretical treatise. *Thin-Walled Struct.* **2015**, *87*, 76–88. [[CrossRef](#)]
26. Yan, P.; Zhang, J.; Fang, Q.; Zhang, Y. Numerical simulation of the effects of falling rock's shape and impact pose on impact force and response of RC slabs. *Constr. Build. Mater.* **2018**, *160*, 497–504. [[CrossRef](#)]
27. Yankelevsky, D.Z.; Karinski, Y.S.; Brodsky, A.; Feldguna, V.R. Dynamic punching shear of impacting RC flat slabs with drop panels. *Eng. Fail. Anal.* **2021**, *129*, 105682. [[CrossRef](#)]
28. Castedo, R.; Santos, A.P.; Alañón, A.; Reifarth, C. Numerical study and experimental tests on full-scale RC slabs under close-in explosions. *Eng. Struct.* **2021**, *231*, 111774. [[CrossRef](#)]
29. Othman, H.; Marzouk, H. An experimental investigation on the effect of steel reinforcement on impact response of reinforced concrete plates. *Int. J. Impact Eng.* **2016**, *88*, 12–21. [[CrossRef](#)]
30. Xiao, Y.; Li, B.; Fujikake, K. Behavior of reinforced concrete slabs under low velocity impact. *ACI Struct. J.* **2017**, *114*, 643–650. [[CrossRef](#)]
31. Jahami, A.; Temsah, Y.; Baalbaki, O.; Darwiche, M.; Al-Rawi, Y.; Al-Ilani, M.; Chaaban, S. Effect of Successive Impact Loads from a Drop Weight on a Reinforced Concrete Flat Slab. *MATEC Web Conf.* **2019**, *281*, 02003. [[CrossRef](#)]
32. Song, H.W.; Wan, Z.M.; Xie, Z.M.; Du, X.W. Axial impact behavior and energy absorption efficiency of composite wrapped metal tubes. *Int. J. Impact Eng.* **2000**, *24*, 385–401. [[CrossRef](#)]
33. Saatci, S.; Batarlar, B. Behavior of Reinforced Concrete Slabs Subjected to Impact Loading. In Proceedings of the 10th International Congress on Advances in Civil Engineering, Ankara, Turkey, 17–19 October 2012.
34. Corbett, G.G.; Reid, S.R.; Johnson, W. Impact loading of plates and shells by free-flying projectiles: A review. *Int. J. Impact Eng.* **1996**, *18*, 141–230. [[CrossRef](#)]
35. Foraboschi, P. Falling mass bearing capacity of reinforced concrete beams. *Eng. Fail. Anal.* **2022**, *138*, 106396. [[CrossRef](#)]
36. Foraboschi, P. Shear Strength of an Anchor Post-Installed into a Hardened Concrete Member. *SSRN Electron. J.* **2022**, *1*, 1–31. [[CrossRef](#)]
37. Foraboschi, P. Strengthening of Reinforced Concrete Beams Subjected to Concentrated Loads Using Externally Bonded Fiber Composite Materials. *Materials* **2022**, *15*, 2328. [[CrossRef](#)]
38. ABAQUS/CAE FEA Program Version 6.15. Concrete Damage Plasticity Model, Explicit Solver, Three Dimensional Solid Element Library, Interactions, Restraints, Keypcard Library; ABAQUS DS-SIMULIA User Manual, France.
39. Hafezolghorani, M.; Hejazi, F.; Vaghei, R.; Jaafar, B.S.M.; Karimzade, K. Simplified damage plasticity model for concrete. *Struct. Eng. Int.* **2017**, *27*, 68–78. [[CrossRef](#)]
40. Lubliner, J.; Oliver, J.; Oller, S.; Onate, E. A plastic-damage model for concrete. *Int. J. Solids Struct.* **1989**, *25*, 299–326. [[CrossRef](#)]
41. International Federation for Structural Concrete. *Fib Model Code for Concrete Structures 2010*; Ernst & Sohn publishing house: Berlin, Germany, 2013.
42. *Structures to Resist the Effects of Accidental Explosions*; Technical Manual, Unified Facilities Criteria UFC 3-340-02; USA Army Corporations of Engineers: Washington, DC, USA, 5 December 2008.
43. Pereira, J.M.; Campos, J.; Lourenco, P.B. Experimental Study on Masonry Infill Walls under Blast Loading. In Proceedings of the 9th International Masonry Conference, Guimarães, Portugal, 7–9 July 2014.
44. Kyei, C.; Braimah, A. Effects of transverse reinforcement spacing on the response of reinforced concrete columns subjected to blast loading. *Eng. Struct.* **2017**, *142*, 148–164. [[CrossRef](#)]
45. Senthil, K.; Thakur, A.; Singh, A.P.; Iqbal, M.A.; Gupta, N.K. Transient dynamic response of brick masonry walls under low velocity repeated impact load. *Int. J. Impact Eng.* **2023**, *174*, 104521. [[CrossRef](#)]
46. Minh, H.L.; Khatir, S.; Wahab, M.A.; Cuong-Le, T. A concrete damage plasticity model for predicting the effects of compressive high-strength concrete under static and dynamic loads. *J. Build. Eng.* **2021**, *44*, 103239. [[CrossRef](#)]
47. Yuen, T.Y.P.; Wen, T.H.; Hung, C.C.; Zhang, H.; Pham, P.A.H.; Deng, Y. An Eigen decomposition-based and mesh-sensitivity reduced constitutive model for nonlinear analysis of concrete structures under non-proportional cyclic loading. *J. Build. Eng.* **2022**, *47*, 103875. [[CrossRef](#)]

Disclaimer/Publisher's Note: The statements, opinions and data contained in all publications are solely those of the individual author(s) and contributor(s) and not of MDPI and/or the editor(s). MDPI and/or the editor(s) disclaim responsibility for any injury to people or property resulting from any ideas, methods, instructions or products referred to in the content.